Exp Brain Res (2012) 222:255–264
DOI 10.1007/s00221-012-3213-6

RESEARCH ARTICLE

Reproducibility and sensitivity of detecting brain activity by simultaneous electroencephalography and near-infrared spectroscopy

Martin Biallas · Ivo Trajkovic · Daniel Haensse · Valentine Marcar · Martin Wolf

Received: 19 September 2011 / Accepted: 28 July 2012 / Published online: 26 August 2012

Abstract The aims were (1) to determine the sensitivity and reproducibility to detect the hemodynamic responses and optical neuronal signals to brain stimulation by near-infrared spectroscopy (NIRS) and evoked potentials by electroencephalography (EEG) and (2) to test the effect of novel filters on the signal-to-noise ratio. This was achieved by simultaneous NIRS and EEG measurements in 15 healthy adults during visual stimulation. Each subject was measured three times on three different days. The sensitivity of NIRS to detect hemodynamic responses was 55.2 % with novel filtering and 40 % without. The reproducibility in single subjects was low. For the EEG, the sensitivity was 86.4 % and the reproducibility 57.1 %. An optical neuronal signal was not detected, although novel filtering considerably reduced noise.

M. Biallas · I. Trajkovic · D. Haensse · M. Wolf
Biomedical Optics Research Laboratory, Division of Neonatology, Department of Obstetrics and Gynecology, University Hospital Zurich, 8091 Zurich, Switzerland

M. Biallas · I. Trajkovic · D. Haensse
Institute for Biomedical Engineering, University of Zurich, 8093 Zurich, Switzerland

M. Biallas (✉) · I. Trajkovic · D. Haensse
ETH Zurich, 8093 Zurich, Switzerland
e-mail: martin.biallas@alumni.ethz.ch

V. Marcar
Institute of Psychology, Neuropsychology, University of Zurich, Zurich, Switzerland

V. Marcar
Dept. Gesundheit, Physiotherapie, ZHAW Zurich University of Applied Sciences, 8401 Winterthur, Switzerland

Keywords Event-related optical signal (EROS) · Near-infrared spectroscopy (NIRS) · Near-infrared imaging (NIRI) · Oxygenated hemoglobin (O2Hb, oxyHb, HbO2) · Deoxygenated hemoglobin (HHb, deoxyHb, HbR) · Hemoglobin · Electroencephalography (EEG) · Evoked potential

Introduction

Functional near-infrared spectroscopy (NIRS) measures non-invasively changes in oxyhemoglobin ($\Delta[O_2Hb]$) and deoxyhemoglobin ($\Delta[HHb]$) concentrations caused by localized cortical activity of the brain. However, the reproducibility of the functional response was assessed rarely in literature (Kono et al. 2007; Plichta et al. 2006).

In vitro experiments on cellular level and invasive in vivo measurements (open skull) have shown that the activation of neurons is accompanied by changes in their optical properties, that is the optical neuronal signal, which can be detected by NIRS (Stepnoski et al. 1991; Rector et al. 2005). This fact is undebated. There is a controversy, whether these optical changes can be detected non-invasively in adult human subjects (Medvedev et al. 2008; Tse et al. 2010; Franceschini and Boas 2004; Steinbrink et al. 2000; Wolf et al. 2003; Steinbrink et al. 2005; Gratton and Fabiani 2010). In non-invasive NIRS measurements, the light has to penetrate superficial tissue such as skin and skull before reaching the brain. For this reason, the net amplitude of the optical neuronal signal is strongly diluted. There is a consensus that the optical neuronal signal is very small compared to the physiological noise level (Wolf et al. 2008). Consequently, since the detection of the optical neuronal signal depends on a sufficient signal-to-noise ratio (SNR) and since the size of the signal cannot

be changed, improvements in SNR must focus on a reduction in the physiological noise, that is, new approaches to filter the NIRS recordings. In this publication, a novel filter for reducing the physiological noise level is applied, and the results are discussed. The aim of this study was to determine (1) the sensitivity of NIRS to detect visually evoked hemodynamic responses, (2) the effect of applying a "double-detector optode least square approach" (DDOLS) (Saager and Berger 2005) to attenuate superficial physiological signal components, (3) the reproducibility of these hemodynamic responses in repeated recordings of each subject, (4) the efficiency of a novel approach "parameter estimation of a model for almost periodic signals" (PEMAPS) to remove the heartbeat in NIRS signals to reduce noise, (5) the sensitivity and reproducibility of optical neuronal signals in NIRS and (6) the sensitivity and reproducibility of evoked potentials in EEG.

Method

Subjects

Fifteen healthy adult subjects (10 male, 5 female, mean age ± SD 29.53 ± 7.89 years) participated in this study. Each subject was measured three times on three different days. Subjects with corrective lenses were asked to wear them during the experiment and were instructed to avoid movement. This study was performed in compliance with the Code of Ethics of the World Medical Association (Declaration of Helsinki) and was approved by the Ethical Committee of the County of Zurich. Written informed consent was obtained from all subjects before inclusion in the study.

Instrumentation

Near-infrared spectroscopy data were acquired using the multichannel continuous wave near-infrared imaging device MCPII (Haensse et al. 2005) with the sensor displayed in Fig. 1. MCPII was configured to measure 11 source/detector combinations, each of 750, 800 and 875 nm resulting in 33 data channels. The term "raw NIRS signal" refers to a single data channel. The sampling rate was 100 Hz per data channel, that is, every 10 ms, 33 samples were acquired by time-multiplexing (Haensse et al. 2005; Haensse 2005).

The sensor was placed on the head such that the electrode's position O_1 (according to the international 10/20 system Jaspers 1958) was located as shown in Fig. 2.

To reduce light attenuation by hair, a stencil of the sensor with holes at all source/detector positions was placed at the appropriate position and fixated tightly with

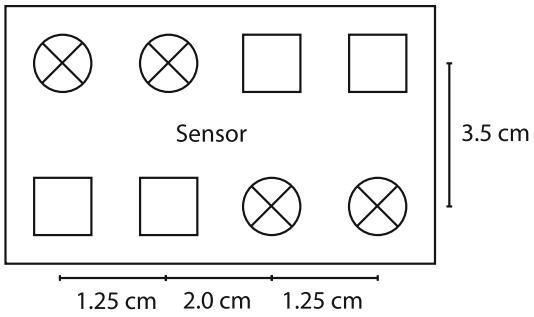

Fig. 1 Geometry of the used light sensor. Light sources/detectors are *circles/squares*

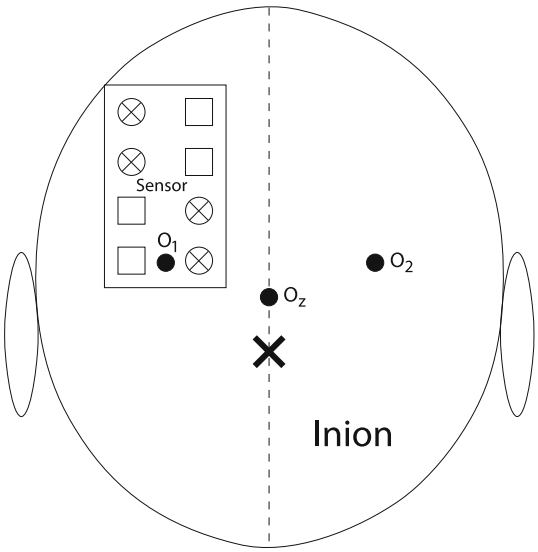

Fig. 2 Sensor's positioning on the back of the subject's head. Electrode O_1 was not placed. EEG analysis was performed on O_2 only

stripes of Velcro. Hair under the stencil's holes was tugged aside by cotton buds. Finally, the sensor was placed over the stencil and attached to the head by bandages.

Electroencephalography data were recorded with MitSar201® using the WinEEG software. Ag/AgCl ring electrodes in conjunction with abrasive paste were used to improve skin conductivity.

Before and after recording, electrode impedances were assured to be below 15 kΩ. Electrodes were positioned according to Jaspers (1958) at O_2, F_3, ground at F_Z and the reference at the earlobe. To minimize electrical interference between the electrodes and the NIRS sensor, MCPII's and MitSar201®'s amplifiers were put on opposite sites of the subject, such that the paths of the electrode leads and the sensor's cable were in opposite directions.

The subject's visual cortex was stimulated by a TFT screen (250 cd/m^2, full on/full off contrast ratio 400:1). A separate computer was attached to this screen and generated synchronizing signals for MCPII and MitSar®.

Protocol

During the experiment, subjects were lying on a table with an u-shaped headrest that permitted unobstructed view to the floor, where a TFT monitor was installed subtending a visual angle of 18.7° × 24.2° for visual stimulation. Stimulation was by black and white dartboard pattern reversals and a black screen during rest intervals programmed in Presentation®. Stimulation intervals and rest intervals were 20 s long. Before the start of an experiment, the frequency of the pattern reversal was adjusted to 1.5 or 2.5 times the heartbeat rate (HBR) to avoid physiological noise caused by the harmonics of the HBR. In addition, if the heart rate is close to the stimulation frequency, this can lead to frequency pulling and synchronization of the heart rate, which may lead to false-positive results in our experience. The frequency of the pattern reversal was varied randomly by ±0.5Hz. The experiment took 20 min inclusively 2-min baseline recording before the first stimulation interval and 1-min baseline after last stimulation interval. During the whole time, the room was kept dark and quiet.

Analysis of hemodynamic response of NIRS

A raw NIRS signal is a time series in which each element is proportional to the measured light intensity. A measurement consists of (1) raw NIRS signals, one for each source/detector/wavelength combination, (2) signals that represent ambient light and (3) event markers. From the 3 raw NIRS signals of the 3 wavelengths from a specific source/detector combination, the sensor's source/detector geometry and the modified Beer–Lambert law (Kocsis et al. 2006; Haensse et al. 2005), 2 new signals can be derived, that is, temporal concentration changes in oxyhemoglobin ($\Delta[O_2Hb]$) and deoxyhemoglobin ($\Delta[HHb]$).

Our setup yielded 11 $\Delta[O_2Hb]$ or $\Delta[HHb]$ signals. Absorption coefficients were taken from the UCL's website,[1] and the differential path length factor (DPF) was set to 8.24, 7.84 and 7.29 at 750, 800 and 875 nm (Zhao et al. 2002).

A customized algorithm implemented in Matlab® evaluated the measurements. This algorithm incorporates deriving $\Delta[O_2Hb]$ and $\Delta[HHb]$ and filtering by DDOLS. The principal idea behind DDOLS is to attenuate superficial and physiological signal components in NIRS data (Saager and Berger 2005). This is achieved by removing changes in a reference channel with short interoptode distance which mostly detects superficial tissue from channels with longer interoptode distance, which are sensitive to deeper tissue. The shortest source/detector distance in this study was 20 mm. All channels were high-pass filtered ($f_c = 0.025$Hz). Exceptional fluctuations in channels, due to movement artifacts, were identified for $\Delta[O_2Hb]$ and $\Delta[HHb]$ signals separately by the following procedure: When a sample in the high-pass-filtered version of the signal (5 pole IIR Butterworth, cutoff frequency 0.5 Hz) exceeded 2 μmol/l, neighboring samples up to 1 s before and 3 s after this sample and the sample itself were excluded from further evaluation.

For each channel, the last 10 s before the stimulation and the period of 10–20 s after the beginning of the stimulation were statistically compared by a paired Wilcoxon test. A hemodynamic response was detected, if the values differed significantly with $p < 0.05$.

EEG data analysis

Only the signal at electrode O_Z was considered. This signal was filtered (bandpass with cutoff frequencies 0.32 and 70 Hz, then notch between 45 and 55 Hz) during recording. When a sample in the signal exceeded 200 μV, neighboring samples and the sample itself were excluded from the evaluation.

In the next step, the signal was detrended by bandpass filtering (5-pole IIR Butterworth).

For stimulation or sham events, the last 50 ms before and the interval from 125 to 175 ms after the stimulation event were compared by a paired Wilcoxon test. A visual activation was detected when the values from the stimulation events differed significantly, and the ones from sham events did not ($p < 0.05$). Testing both types of events prevents the detection of false-positive activations caused by electromagnetic interference.

Filtering the heartbeat by PEMAPS

The heartbeat component in raw NIRS signals is a tremendous source of noise in the analysis of the optical neuronal signal, because changes in $\boldsymbol{o}$ due to the heartbeat are considerably larger than the expected size of the optical neuronal signal (Gratton and Corballis 1995). The aim was to estimate the pure heartbeat component and to subtract it from the raw NIRS signal.

Since there are sharp peaks in the heartbeat, a simple low-pass filter will not work (Trajkovic et al. 2009); thus, we used the method for modeling and adaptive filtering of oscillatory components called Parameter Estimation of a Model for Almost Periodic Signals (PEMAPS) (Trajkovic et al. 2012), which is summarized here.

The heartbeat component is not strictly periodic; it can be characterized as "almost periodic." In an almost periodic signal, the period length and the signal shape drift

[1] http://www.medphys.ucl.ac.uk/research/borl/research/NIR_topics/spectra/spectra.htm.

over time (Trajkovic et al. 2009). Such a signal can be described by a "Fourier series" with time-variant fundamental frequency (related to the varying period length) and time-variant coefficients (related to the varying signal shape). In essence, PEMAPS iteratively estimates the coefficients and the phase of the time-variant Fourier series for each sample in the NIRS signal. Thereby, the energy of the residual signal, which is the NIRS signal minus the estimated heartbeat component from the previous iteration step, is minimized. An in-depth description of the PEMAPS is given in "appendix" (Fig. 3).

Analysis of optical neuronal responses

The analysis consists of the following steps.

1. Estimating the heartbeat component in each data channel by PEMAPS (section "Filtering the heartbeat by PEMAPS"). For all subjects, PEMAPS was set up with $K \triangleq 15$ in (1), message damping factors for harmonic indices $k = 0 : \gamma \triangleq 0.97, k > 0 : \gamma \triangleq 0.945$ (see Trajkovic 2010, section "The new coefficient estimator"); furthermore, $\hat{\Omega} \triangleq 0.0595$ rad. (see paragraph after Eq. 7), regularization strength $\eta \triangleq 0.0005$ and $\sigma_k^{*2} = 0.00003$ (see Trajkovic 2010, section "The new coefficient estimator"), and the variance of the "$\mathcal{N}$"-node in all factor graphs (see Trajkovic 2010) $\sigma^2 \triangleq 600$. These values were determined empirically.
2. Calculating the corresponding optical density signal from each data channel: $\boldsymbol{o} \triangleq \frac{\log(\boldsymbol{y}-\hat{\boldsymbol{x}}+\hat{\boldsymbol{A}}_{0,-})}{\mathrm{DPF}(\lambda)\cdot d}$ with geometric source/detector distance d (in cm), wavelength λ, $\boldsymbol{y}$ and $\hat{\boldsymbol{x}}$ as defined in section "Filtering the heartbeat by PEMAPS," and a slow trend $\hat{\boldsymbol{A}}_{0,-}$. The latter was computed separately with $\gamma \triangleq 0.999$ to minimize the influence of the heartbeat's fundamental frequency.
3. Bandpass filtering of $\boldsymbol{o}$ with cutoff frequencies <5 and 40 Hz. The low cutoff frequency was manually calculated for each subject to ensure that it was lower than the varying frequency of the pattern reversals in the visual stimulation (see section "Protocol"). The higher cutoff frequency was chosen empirically to attenuate irrelevant frequencies.
4. Subtracting the mean value of each segment (stimulus and sham) in $\boldsymbol{o}$.
5. Applying a moving variance window (1 s width) to identify segments which exceed the threshold of two times the variance of all segments. In each data channel, this procedure identified and rejected stimulation (sham) events with outliers caused by movement artifacts.
6. Computing two average segments for each data channel: one for all accepted segments during stimulation and one for all accepted segments during sham. These resulting segments cover a time interval from 10 ms before and 270 ms after stimulation, and sham, respectively.

The shape of optical neuronal responses is unknown. Thus, each sample in the 200-ms-long average segment was checked whether it significantly differs from 0 (t test, $p < 0.05$). This was done for all source/detector/wavelength combinations and subjects.

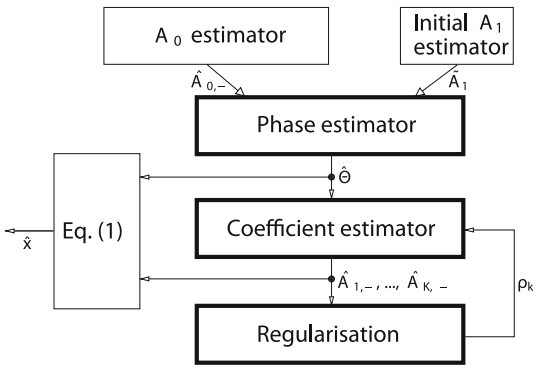

Fig. 3 This diagram visualizes the principle of the PEMAPS approach and its building blocks

Results

Hemodynamic response

In some measurements, there was no activation in the EEG signal, and we concluded that in these subjects, the stimulation was not successful. The following results are based on measurements, which showed an activation in the EEG. Using DDOLS, a significant hemodynamic response reflecting brain activation was found in 55.2 % of the measurements (16 HR in 29 recordings). Without DDOLS, it was lower, that is 36.8 % (14 HR in 38 recordings). In 40.0 % (based on 5 subjects), a significant hemodynamic response was found in three repeated measurements with DDOLS and in 12.5 % out of 8 subject without DDOLS. An activation was found at least twice with DDOLS in 30.0 % (based on 10 subjects) and in 26.7 % (based on 15 subjects) without DDOLS. At least one single occurrence of a significant hemodynamic response was found in 78.6 % out of 14 subjects with DDOLS and 60.0 % out of 15 subjects without DDOLS. Table 1 displays the findings for all measurement separately. Figure 4 shows an example of a significant hemodynamic response.

Table 1 Overview of subjects and result of analysis

Subject index	Gender	Age	Recording index	No. of days since rec. A	*p* value HR w/o DDOLS	HR Δmean [μmol/l] w/o DDOLS	*p* value HR w DDOLS	HR Δmean [μmol/l] w DDOLS	VEP Δmean [μV]
1	F	21	A	0	–	–	0.0316	0.0192 ± 0.0082	5.8 ± 0.4
			B	1	–	–	0.0207	0.0444 ± 0.0169	7.1 ± 0.2
			C	2	–	–	0.0495	−0.0242 ± 0.0116	2.5 ± 0.4
2	F	25	A	0	0.0313	0.7178 ± 0.0648	n.a.	n.a.	−7.3 ± 0.3
			B	9	–	–	n.a.	n.a.	−8.5 ± 0.3
			C	98	0.0060	0.0838 ± 0.0265	0.0073	0.0723 ± 0.0268	2.8 ± 0.3
3	F	25	A	0	–	–	–	–	4.3 ± 0.3
			B	3	0.0300	−0.0274 ± 0.0161	0.0011	0.0203 ± 0.0056	3.8 ± 0.3
			C	4	–	–	–	–	1.9 ± 0.3
4	F	23	A	0	0.0125	−0.0313 ± 0.0119	4.4493×10^{-5}	0.0390 ± 0.0069	3.5 ± 0.3
			B	3	0.0068	−0.0280 ± 0.0092	0.0010	−0.0333 ± 0.0088	6.0 ± 0.3
			C	5	0.0333	−0.0216 ± 0.0107	0.0270	0.0078 ± 0.0033	6.0 ± 0.4
5	F	38	A	0	0.0059	0.0999 ± 0.0293	n.a.	n.a.	6.7 ± 0.4
			B	7	0.0020	0.6141 ± 0.0758	n.a.	n.a.	6.0 ± 0.5
			C	60	–	–	0.0449	−0.0430 ± 0.0216	7.0 ± 0.5
6	M	33	A	0	–	–	0.0230	0.0834 ± 0.0339	5.5 ± 0.2
			B	1	–	–	–	–	4.6 ± 0.2
			C	2	–	–	–	–	6.1 ± 0.9
7	M	28	A	0	–	–	–	–	–
			B	1	0.0057	−0.1064 ± 0.0334	n.a.	n.a.	8.4 ± 0.3
			C	7	–	–	–	–	5.6 ± 0.4
8	M	25	A	0	–	–	–	–	2.8 ± 0.3
			B	1	–	–	–	–	–
			C	2	–	–	0.0117	0.0346 ± 0.0121	2.9 ± 0.4
9	M	25	A	0	–	–	–	–	7.6 ± 0.3
			B	4	0.0148	−0.0692 ± 0.0281	0.0077	−0.0308 ± 0.0106	10.8 ± 0.3
			C	6	–	–	–	–	8.0 ± 0.5
10	M	27	A	0	–	–	–	–	3.5 ± 0.3
			B	7	–	–	–	–	2.4 ± 0.4
			C	8	–	–	–	–	–
11	M	28	A	0	–	–	n.a.	n.a.	–
			B	80	–	–	–	–	3.4 ± 0.3
			C	83	0.0117	0.1980 ± 0.0658	–	–	10.2 ± 0.3
12	M	28	A	0	0.0020	−0.0715 ± 0.0140	n.a.	n.a.	8.2 ± 0.2
			B	1	0.0087	0.0873 ± 0.0397	n.a.	n.a.	n.a.
			C	8	–	–	0.0036	0.0751 ± 0.0285	18.3 ± 0.3
13	M	29	A	0	0.0093	−0.0563 ± 0.0189	0.0028	0.0704 ± 0.0202	–
			B	1	–	–	0.0256	0.0399 ± 0.0171	5.5 ± 0.1
			C	4	–	–	0.0449	0.0472 ± 0.0237	5.0 ± 0.2
14	M	38	A	0	–	–	–	–	9.0 ± 0.2
			B	1	–	–	n.a.	n.a.	7.0 ± 0.2
			C	3	–	–	0.0185	0.0174 ± 0.0070	6.5 ± 0.2
15	M	50	A	0	0.0385	−0.1750 ± 0.0725	n.a.	n.a.	6.2 ± 0.3
			B	16	–	–	n.a.	n.a.	–
			C	43	0.0461	−0.1208 ± 0.0543	n.a.	n.a.	5.9 ± 0.4

HR hemodynamic response

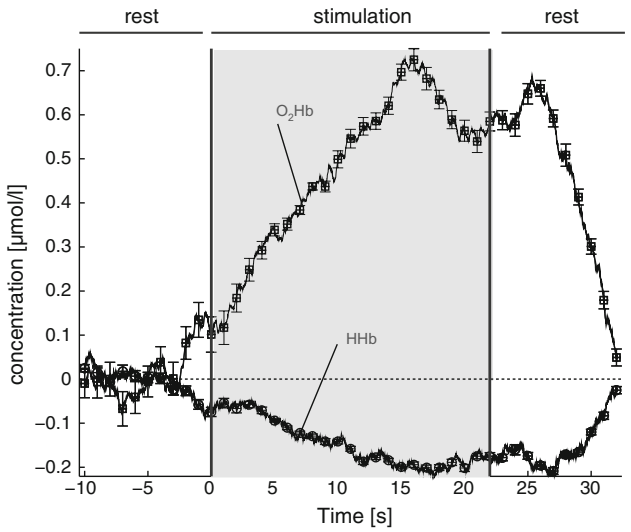

Fig. 4 A hemodynamic response that shows an increase in $\Delta[O_2Hb]$ and decrease in Δ[HHb]. It was derived by calculating, samplewise, the median of all accepted stimulation intervals in the $\Delta[O_2Hb]$ and Δ[HHb] signal. Both *curves* were smoothed by a moving average filter (window length 5 s). The *gray area* indicates the stimulation period, and the *error bars* represent the standard error of the mean

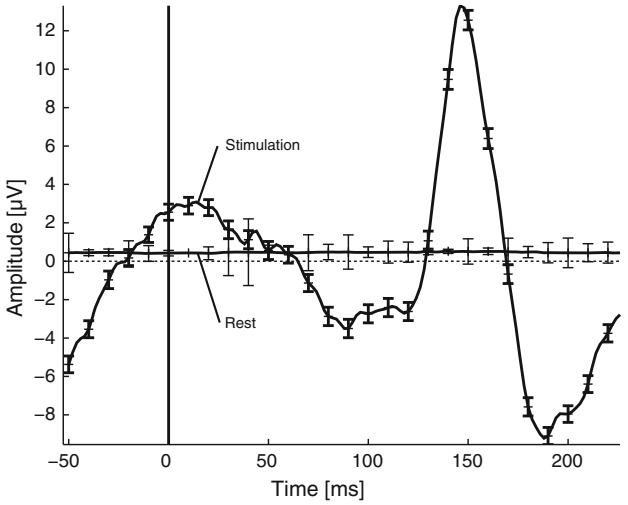

Fig. 5 Depicted are two EEG signals: one is the block average during stimulation and the other during sham. The response in the form of VEP is clearly visible as a peak at 150 ms. The pattern reversal happened at 0 ms (*vertical line*)

Visual evoked potential (VEP)

An exemplary VEP signal is depicted in Fig. 5. Assuming that stimulation was successful in all valid measurements yields a sensitivity of 86.4 %. Reproducibility was found in three repeated measurements in 57.1 % of all 14 subjects.[2] In all 15 subjects, a VEP was detected twice. No subject showed a VEP only once or not at all in the repeated measurements.

Optical neuronal signal

The histograms in Fig. 6 show the number of significances (y-axis) normalized by the total number of data samples at each point in time (x-axis) after the stimulation. The data are shown for the analysis without (Fig. 6a, b) and with PEMAPS (Fig. 6c, d) and for data reflecting real stimulations (Fig. 6a, c) and sham (Fig. 6b, d). For a significance level of $p < 0.05$, we would expect a proportion of 0.05 of the signals to be significant just by chance. Would the optical neuronal response behave like the VEP and feature a peak at 150 ms, the number of detected significances should increase at 150 ms for example. In case of a delay between the onset of a VEP and the optical neuronal response, the increase of significances would occur with this delay. However, no increase of significances occurred in the analysis. Without PEMAPS, many significances were found similarly for stimulation and rest. Thus, PEMAPS was able to reduce the number of false positives considerably. Comparing Fig. 6c, d shows that the pattern of significant samples is similar during stimulation and rest meaning that the optical neuronal signal was not detected.

The magnitude of changes in the optical density of a data channel needed to be induced by an optical neuronal signal in order to be detected can be derived from Fig. 6. The latter displays the noise level of the measurements with and without PEMAPS. PEMAPS particularly decreased the SEMs of the data channels with already small SEMs ($<10^{-7}$).

Histograms as in Figs. 6 and 7 were plotted for each distance/wavelength combination separately to test whether any of the specific wavelengths or distances may be particularly sensitive to detect an optical neuronal signal. In general, these histograms showed a higher influence of the heartbeat on the short distance and long wavelength (20 mm, 875 nm). However, the histograms looked similar for stimulation and rest, and thus, none of the specific wavelengths or distances were sensitive enough to detect the optical neuronal signal.

Discussion

Hemodynamic response

In regard to DDOLS, the shortest interoptode distance was saturated (too much light) in several measurements, such that DDOLS could not be applied.[3] Our shortest

[2] One measurement could not be evaluated. Therefore, this subject is not included in the total number of subjects.

[3] When DDOLS could not be applied, the columns are marked by "n.a." in Table 1.

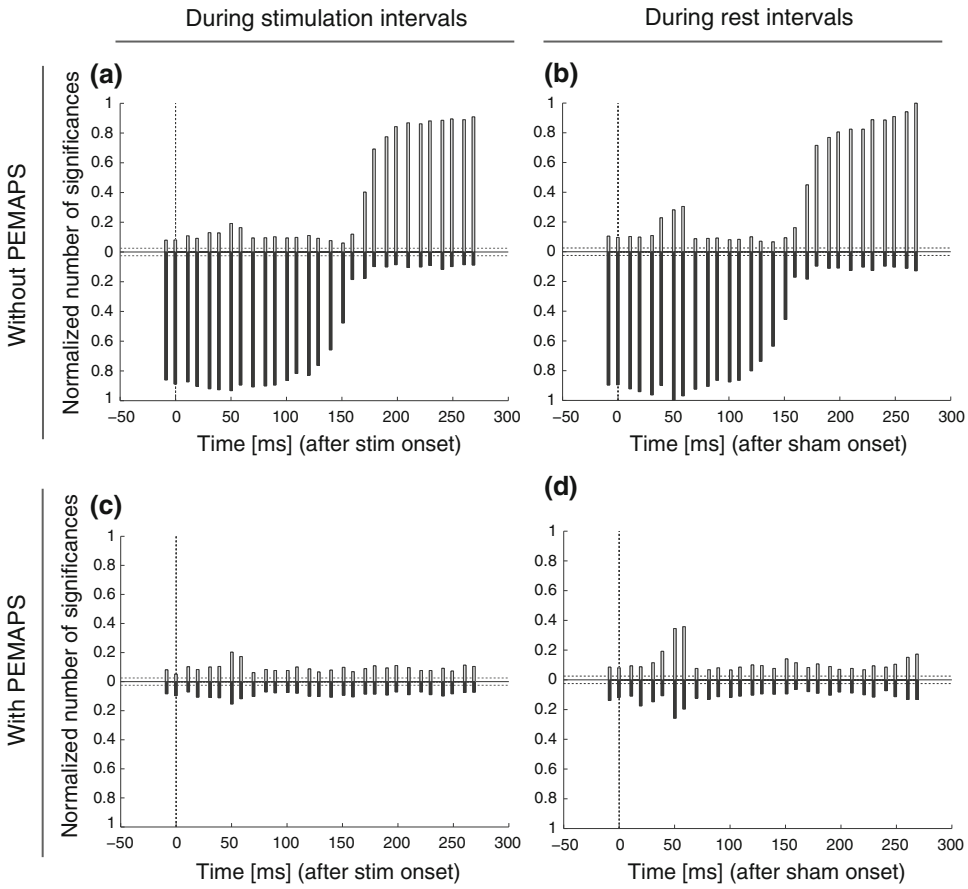

Fig. 6 Distribution of significant ($p < 0.05$) samples in the block average segments over all data channels and measurements. Occurrences are normalized, so that 0.05 is the value random significances can be responsible for. The *black broken bar* at time 0 ms marks the beginning of a stimulation event. Since the occurrences are divided into two groups, significant negative deviation of mean in *black* and significant positive deviation of mean in *gray*, the indicated threshold for randomly occurring significances was set to 0.05/2. For better visualization, number of occurrences of significant negative deviations is depicted in quadrant four. The number of significances in plots **a** and **b** is higher than the number of significances in plots **c** and **d**, showing the effectiveness of PEMAPS in reducing false-positive data, importance of proper heartbeat removal and the necessity of comparing stimulation and rest intervals

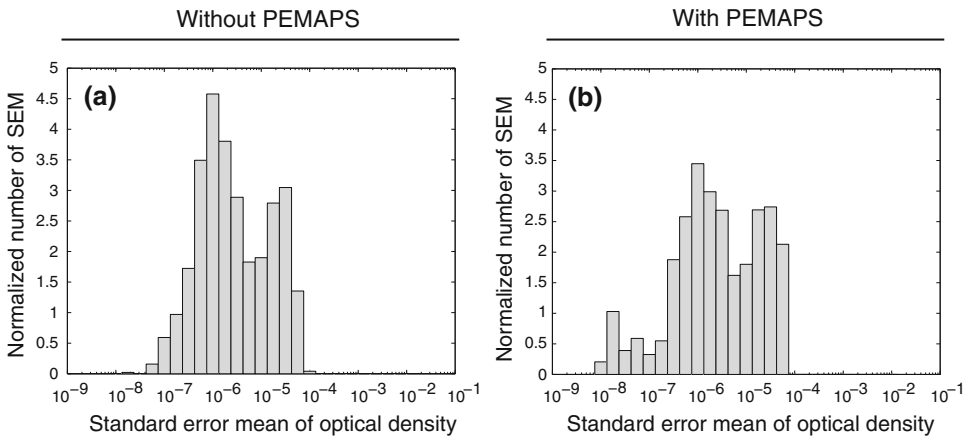

Fig. 7 Depicted is the distribution of standard errors of the mean (SEM) of all measured data channels. The histogram displays the number of occurrences of a range of SEMs normalized to the number of data channels. PEMAPS increased the number of occurrences of lower SEMs

interoptode distances of 20 mm was somewhat larger than the 1 mm to 13 mm used in Saager and Berger (2005). Despite these limitations, DDOLS increased the sensitivity from 36.8 to 55.2 %. When longer source/detector distances are used for DDOLS ' reference channel as in our case, it is advisable to check the reference channels for activation and account for it in analysis. If activation is present, DDOLS should not be used, because it will remove also the activation signal from other channels[4]. The sensitivity could be increased further with an improved optode, which offers also shorter interoptode distances as suggested by Saager and Berger.

[4] This is the case in the following 3 recordings: subject 7, recording B, and in subject 12, recordings A and B.

Possible reasons for this may be imprecision in locating the position O_1 (Echallier et al. 1992), repositioning inaccuracy for the sensor between measurements ($\sim \pm 5$ mm), and the area covered by the light sensor. As outlined in Plichta et al. (2006), location of significantly activated brain areas was only in 55 % identical within a subject over 2 NIRS measurements. This is confirmed by Machielsen et al. (2000) with MRI.

Visual evoked potential

A VEP was found in 86.4 % of 44 measurements. One dataset could not be processed due to instrumental artifacts.

Surprisingly, a VEP could not be detected more frequently as suggested by the literature (Benavente et al. 2005; Sarnthein et al. 2009). This may be due to the higher electrode/skin impedances accepted in our study in comparison with other studies (Ikeda et al. 1998; Török et al. 1992; Odom et al. 2004). This favors the pick up of electromagnetic interference and may obscure small VEPs. A further difference to literature is utilizing only a single channel as reference. Another reason may be that the stimulation was not successful. In our opinion, this is the most probable reason.

Optical neuronal signal

Despite low noise levels (Fig. 7b), no optical neuronal signal was detected (Fig. 6). The idea behind the histograms in Fig. 6c, d is to compare random significances to possible event-related significances. The random signals were generated by adding stimulation markers during the rest periods when no stimulation occurred. These random signals were analyzed in the same way as signals during stimulation, that is, they include the same instrumental and methodical artifacts. At significance level of $p < 0.05$, it is expected that 5 % of the data points are significant just by chance. In Fig. 6a, b higher incidences of significant data points are shown. These higher numbers are the same for real (Fig. 6a) and sham (Fig. 6b) stimulation clearly indicating that the higher incidence is due to methodological problems and that these incidences are false positive. This illustrates the importance of an effective suppression of the heartbeat component. Without such a filter, the data in the block-averaged segments are dominated by artifacts (Fig. 6a, b). This also demonstrates the importance of proper controls to interpret the results correctly, because otherwise, if only Fig. 6a was observed, one may erroneously conclude that optical neuronal signals were present.

In Fig. 6c, d, the data after removing the heartbeat component by PEMAPS, the incidence of significances reaches a level closer to 5 %, which corresponds to the level expected to be significant by chance.

The peaks at about 50 ms after stimulation onset are again similar for real stimulation and sham and thus do not represent a specific stimulation response. They are probably due to an instrumental artifact.

As already stated, the figures demonstrate the need to compare stimulation and rest intervals to distinguish between real signals and artifacts.

Figure 7 displays how noise, that is the SEM of optical densities, spreads over several magnitudes. Obviously, there are more and less noisy data channels that depend on the light intensity at the detector, that is, the more light, the higher the SNR, and the level of physiological noise. For shorter distances, the SNR is higher, since more light is detected. The percentile P_{20} of the histogram in Fig. 7b is at $\mathrm{SEM}(\boldsymbol{o}) = 4.8 \times 10^{-7}$. This means that in 20 % of the data channels, an optical neuronal signal with an amplitude of $1.96 \times \mathrm{SEM}(\boldsymbol{o}) \approx 9.41 \times 10^{-5}$ % would have been detected with a probability of 95 %. Optical neuronal signals with light intensity changes of 0.05 %, as seen in the literature (Wolf et al. 2008), would have been detected.

Conclusion

Applying DDOLS increases the sensitivity of NIRS to detect hemodynamic responses from 36.8 to 55.2 %. The reproducibility of the hemodynamic response in a single subject was low (40 %). EEG had a high sensitivity of 86.4 % and a reproducibility of 55.2 %. Raw data with low SEM are further enhanced by PEMAPS. Without PEMAPS, artifactual signals are obtained. We detected no optical neuronal signal despite 20 % of the signals having extremely low noise (4.8×10^{-5} %). The results underline the importance of a proper control to avoid false-positive conclusions, that is, as significant events are detected during both stimulation and sham (or rest) periods, it is important to use proper sham periods as control.

Acknowledgments The authors gratefully acknowledge the funding of the Swiss National Science Foundation. Many thanks to Felix Scholkmann for help with the figures.

Appendix: Details of PEMAPS

Under this assumption that the heartbeat component is a Fourier series with time-variant fundamental frequency (related to the varying period length) and time-variant coefficients (related to the varying signal shape), the sampled version of the real-valued heartbeat component $x_1, x_2, \ldots$ is given as

$$x_n = \mathrm{Re}\left(\sum_{k=1}^{K} A_{k,n} e^{jk\Theta_n}\right) \tag{1}$$

with coefficients $A_{0,n} \in \mathbb{R}, A_{1,n}, \ldots, A_{K,n} \in \mathbb{C}$, phase $\Theta_n \in [0, 2\pi]$, finite number of frequencies K and

$$A_{k,n+1} \approx A_{k,n}, \tag{2}$$

$$\Theta_{n+1} = (\Theta_n + \Omega_n) \bmod 2\pi, \tag{3}$$

$$\Omega_{n+1} \approx \Omega_n. \tag{4}$$

Equation (4) expresses the varying heart rate; (2) expresses the varying beat shape. Let the raw NIRS signal vector $\boldsymbol{y} = (y_1, \ldots, y_N)$ be a noisy, trended version of $\boldsymbol{x} = (x_1, \ldots, x_N)$ where N is the signal length. Specifically,

$$\boldsymbol{y} = \boldsymbol{A}_{0,-} + \boldsymbol{x} + \boldsymbol{Z} \tag{5}$$

where $\boldsymbol{Z} = (Z_1, \ldots, Z_N)$ is discrete time white Gaussian noise, and $\boldsymbol{A}_{0,-} = (A_{0,1}, \ldots, A_{0,N})$ models changes slower than the heartbeat and thus is omitted in (1). We will use the vectors $\boldsymbol{A}_{k,-} = (A_{k,1}, \ldots, A_{k,N})$ for $k = 0, \ldots, K$ and decorate estimates with a hat (e.g. $\hat{C}$ is an estimate of C).

Given $\boldsymbol{y}$, the objective is to estimate the phases $\boldsymbol{\Theta} \triangleq (\Theta_1, \ldots, \Theta_N), K$ and the coefficient vectors $\boldsymbol{A}_{1,-}$, $\ldots$, $\boldsymbol{A}_{K,-}$ such that

$$\sum_{n=1}^{N} (y_n - \hat{x}_n - \hat{A}_{0,n})^2.$$

is minimal, where $\hat{x}_n$ is the reconstructed signal by applying the estimates in (1).

The estimation algorithm consists of several building blocks (see Fig. 3). Initially, the "A_0 estimator" estimates the slow trend $\boldsymbol{A}_{0,-}$ by a one-time procedure similar to low-pass filtering and based on $\boldsymbol{y}$ only.

In the heartbeat component, most of the energy, apart from the noise, lies in the fundamental frequency coefficient $\boldsymbol{A}_{1,-}$. Thus, a first rough estimate of the heartbeat component is a complex sinusoid with constant complex magnitude. The "Initial A1 estimator" block makes an estimate $\tilde{A}_1$ of this magnitude such that the sinusoid has approximately the same energy as $\boldsymbol{y} - \hat{\boldsymbol{A}}_{0,-}$.

The "Phase estimator" calculates the final estimate $\hat{\boldsymbol{\Theta}}$ of $\boldsymbol{\Theta}$ based on estimates $\hat{\boldsymbol{A}}_{0,-}$ and $\tilde{A}_1$ and (1) with $K = 1$ parameterized as

$$\begin{aligned} x_n &= \mathrm{Re}\left(\tilde{A}_1 \cdot e^{j\Theta_n}\right) \\ &= \mathrm{Re}(\tilde{A}_1)\cos(\Theta_n) - \mathrm{Im}(\tilde{A}_1)\sin(\Theta_n) \\ &= \hat{\boldsymbol{A}}_1 \cdot \boldsymbol{C}_n \end{aligned} \tag{6}$$

with constant vector $\hat{\boldsymbol{A}}_1 = \left(\mathrm{Re}(\tilde{A}_1), -\mathrm{Im}(\tilde{A}_1)\right)$, state vector $\boldsymbol{C}_n = (\cos(\Theta_n), \sin(\Theta_n))^T$ and state transition

$$\boldsymbol{C}_n = \mathrm{rot}(\hat{\Omega}) \cdot \boldsymbol{C}_{n-1} + \boldsymbol{U}_n \tag{7}$$

where

$$\mathrm{rot}(\Omega) = \begin{pmatrix} \cos(\hat{\Omega}) & -\sin(\hat{\Omega}) \\ \sin(\hat{\Omega}) & \cos(\hat{\Omega}) \end{pmatrix}$$

is a rotation matrix, and $\hat{\Omega}$ is an a priori estimate of Ω_n in (4). $\hat{\Omega}$ is derived using the formula in Trajkovic et al. (2009), section "Optical neuronal signal," paragraph 4 and assuming a typical heart rate depending on the subject, for example $H = 80$ bpm for adults. Since $\hat{\Omega}$ is fixed, despite the fact that the heart rate varies considerably depending on various factors, uncertainty, that is two-dimensional zero-mean white Gaussian noise $\boldsymbol{U}_n$, is added to the rotated state in (7). This addition of noise defines (4).

The estimate $\hat{\boldsymbol{C}}_n$ of $\boldsymbol{C}_n$ is made as

$$\hat{\boldsymbol{C}}_n = \arg\max_{\boldsymbol{C}_n} f(\boldsymbol{C}_n \,|\, \boldsymbol{A}_{0,-}, \tilde{A}_1, \boldsymbol{y}). \tag{8}$$

The function f in (8) (1) comprises (5), (6) and (7) and (2) is derived with the message passing algorithm described in Trajkovic et al. (2012), section "Method."

Each estimate $\hat{\Theta}_n$ in $\hat{\boldsymbol{\Theta}}$ is made as

$$\hat{\Theta}_n = \arctan\frac{\hat{\boldsymbol{C}}_n(2)}{\hat{\boldsymbol{C}}_n(1)} \tag{9}$$

with $\hat{\boldsymbol{C}}_n(i)$ denoting the i-th entry of the vector $\hat{\boldsymbol{C}}_n$.

The "Coefficient estimator" calculates the full set of coefficient estimates $\hat{\boldsymbol{A}}_{1,-}, \ldots, \hat{\boldsymbol{A}}_{K,-}$. Each estimate $\hat{A}_{k,n}$ of $A_{k,n}$ is calculated based on the estimates $\hat{\boldsymbol{A}}_{k-1,-}, \ldots, \hat{\boldsymbol{A}}_{0,-}, \hat{\boldsymbol{\Theta}}$ and $\boldsymbol{y}$ as

$$\hat{\boldsymbol{A}}_{k,n} = \arg\max_{A_{k,n} \in \mathbb{C}} g(A_{k,n} | \hat{\boldsymbol{A}}_{k-1,-}, \ldots, \hat{\boldsymbol{A}}_{0,-}, \hat{\boldsymbol{\Theta}}, \boldsymbol{y}) \tag{10}$$

for increasing k. The function g in (10) (i) comprises (1), (2) and the assumption of white Gaussian noise in (5) and (ii) is derived with the message passing algorithm described in Trajkovic (2010), section "The new coefficient estimator."

The "Regularization" block is used to iteratively derive the number of harmonics K in (1) as described in Trajkovic et al. (2012), at the end of section "Method."

The "Eq. (1)" block reconstructs the heartbeat component by applying the estimates $\hat{\boldsymbol{A}}_{1,-}, \ldots, \hat{\boldsymbol{A}}_{K,-}$ and $\hat{\boldsymbol{\Theta}}$ in (1).

References

Benavente I, Tamargo P, Tajada N, Yuste V, Oliván M (2005) Flash visually evoked potentials in the newborn and their maturation during the first six months of life. Doc Ophthalmol

110(2):255–263. doi:10.1007/s10633-005-0818-0, http://dx.doi.org/10.1007/s10633-005-0818-0

Echallier J, Perrin F, Pernier J (1992) Computer-assisted placement of electrodes on the human head. Electroencephalogr Clin Neurophysiol 82(2):160–163. doi:10.1016/0013-4694(92)90161-A, http://www.sciencedirect.com/science/article/B6SYX-482RBC6-D5/2/0491640708cb970c66a55d84c181ee0d

Franceschini M, Boas D (2004) Noninvasive measurement of neuronal activity with near-infrared optical imaging. Neuroimage 21(1):372–386

Gratton G, Corballis P (1995) Removing the heart from the brain: compensation for the pulse artifact in the photon migration signal. Psychophysiology 32(3):292–299

Gratton G, Fabiani M (2010) Fast optical imaging of human brain function. Front Hum Neurosci 4:52

Haensse D, Szabo P, Brown D, Fauchère JC, Niederer P, Bucher HU, Wolf M (2005) A new multichannel near infrared spectrophotometry system for functional studies of the brain in adults and neonates. Opt Express 13(12):4525–4538. http://www.opticsexpress.org/abstract.cfm?URI=oe-13-12-4525

Haensse DV (2005) Changes in cerebral oxygenation in response to various stimuli in newborns as measured by functional near-infrared spectroscopy. PhD thesis, ETH Zurich, diss. ETH No. 16356

Ikeda H, Nishijo H, Miyamoto K, Tamura R, Endo S, Ono T (1998) Generators of visual evoked potentials investigated by dipole tracing in the human occipital cortex. Neuroscience 84(3):723–739. doi:10.1016/S0306-4522(97)00569-1, http://www.sciencedirect.com/science/article/B6T0F-3TDPWM5-8/2/4ad7fa3564d376c4bb74d2f3037bacfe

Jaspers HH (1958) Report of the committee on methods of clinical examination in electroencephalography: 1957. Electroencephalogr Clin Neurophysiol 10(2):370–375. doi:10.1016/0013-4694(58)90053-1, http://www.sciencedirect.com/science/article/B6SYX-482YFXP-2S/2/86bdd4bf9cfe6840aec22a5482f1ee66

Kocsis L, Herman P, Eke A (2006) The modified Beer–Lambert law revisited. Phys Med Biol 51:N91

Kono T, Matsuo K, Tsunashima K, Kasai K, Takizawa R, Rogers MA, Yamasue H, Yano T, Taketani Y, Kato N (2007) Multiple-time replicability of near-infrared spectroscopy recording during prefrontal activation task in healthy men. Neurosci Res 57(4):504–512. doi:10.1016/j.neures.2006.12.007, http://www.sciencedirect.com/science/article/B6T0H-4MMPNDG-1/2/21bd601882b23e3aa350f823c5f03345

Machielsen W, Rombouts S, Barkhof F, Scheltens P, Witter M (2000) Fmri of visual encoding: reproducibility of activation. Hum Brain Mapp 9(3):156–164

Medvedev AV, Kainerstorfer J, Borisov SV, Barbour RL, VanMeter J (2008) Event-related fast optical signal in a rapid object recognition task: Improving detection by the independent component analysis. Brain Res 1236:145–158. doi:10.1016/j.brainres.2008.07.122, http://www.sciencedirect.com/science/article/B6SYR-4T6CTR7-6/2/b70eca0903fa2f4a6593dea0005a3904

Odom JV, Bach M, Barber C, Brigell M, Marmor MF, Tormene AP, Holder GE, Vaegan (2004) Visual evoked potentials standard (2004). Doc Ophthalmol 108(2):115–123. doi:10.1023/B:DOOP.0000036790.67234.22, http://dx.doi.org/10.1023/B:DOOP.0000036790.67234.22

Plichta M, Herrmann M, Baehne C, Ehlis AC, Richter M, Pauli P, Fallgatter A (2006) Event-related functional near-infrared spectroscopy (fnirs): are the measurements reliable? Neuroimage 31(1):116–124. doi:10.1016/j.neuroimage.2005.12.008, http://www.sciencedirect.com/science/article/B6WNP-4J55639-1/2/e922aa2ff54ca34ae1ecd8faf70390c8

Rector DM, Carter KM, Volegov PL, George JS (2005) Spatio-temporal mapping of rat whisker barrels with fast scattered light signals. Neuroimage 26(2):619–627. doi:10.1016/j.neuroimage.2005.02.030, http://www.sciencedirect.com/science/article/B6WNP-4FX23HF-2/2/199499aa1100bc547fe864de8cb6f4c7

Saager R, Berger A (2005) Direct characterization and removal of interfering absorption trends in two-layer turbid media. J Opt Soc Am A 22(9):1874–1882

Sarnthein J, Andersson M, Zimmermann MB, Zumsteg D (2009) High test-retest reliability of checkerboard reversal visual evoked potentials (vep) over 8 months. Clin Neurophysiol 120(10):1835–1840. doi:10.1016/j.clinph.2009.08.014, http://www.sciencedirect.com/science/article/B6VNP-4X7PPTK-3/2/b53128d8df48cb41b259425acb0e7044

Steinbrink J, Kohl M, Obrig H, Curio G, Syr F, Thomas F, Wabnitz H, Rinneberg H, Villringer A (2000) Somatosensory evoked fast optical intensity changes detected non-invasively in the adult human head. Neurosci Lett 291(2):105–108. doi:10.1016/S0304-3940(00)01395-1, http://www.sciencedirect.com/science/article/B6T0G-414N3J2-D/2/cd1ba920491d3535629ca44dfc6fec7a

Steinbrink J, Kempf F, Villringer A, Obrig H (2005) The fast optical signal—robust or elusive when non-invasively measured in the human adult. Neuroimage 26(4):996–1008

Stepnoski R, LaPorta A, Raccuia-Behling F, Blonder G, Slusher R, Kleinfeld D (1991) Noninvasive detection of changes in membrane potential in cultured neurons by light scattering. Proc Natl Acad Sci USA 88(21):9382

Török B, Meyer M, Wildberger H (1992) The influence of pattern size on amplitude, latency and wave form of retinal and cortical potentials elicited by checkerboard pattern reversal and stimulus onset-offset. Electroencephalogr Clin Neurophysiol/Evoked Potentials Sect 84(1):13–19. doi:10.1016/0168-5597(92)90063-H, http://www.sciencedirect.com/science/article/B6SYY-482XXNH-8P/2/7c838caf63c4c50d92cb2ddf11066cc1

Trajkovic I (2010) Modelling and filtering almost periodic signals by time-varying fourier series with application to near-infrared spectroscopy. PhD thesis, ETH Zurich, http://e-collection.library.ethz.ch/eserv/eth:2881/eth-2881-01.pdf, diss. ETH No. 19420

Trajkovic I, Reller C, Wolf M, Loeliger H (2009) Modelling and filtering almost periodic signals by time-varying fourier series with application to near-infrared spectroscopy. In: Proceedings of 17th European Signal Processing Conference (EUSIPCO), pp 632–636

Trajkovic I, Reller C, Wolf M (2012) Modelling and filtering of physiological oscillations in near-infrared spectroscopy by time-varying fourier series. In: Wolf M, Bucher HU, Rudin M, Van Huffel S, Wolf U, Bruley DF, Harrison DK (eds) Oxygen transport to tissue XXXIII, advances in experimental medicine and biology, vol 737. Springer, US, pp 307–313. http://dx.doi.org/10.1007/978-1-4614-1566-4_45

Tse CY, Gordon BA, Fabiani M, Gratton G (2010) Frequency analysis of the visual steady-state response measured with the fast optical signal in younger and older adults. Biol Psychol 85(1):79–89. doi:10.1016/j.biopsycho.2010.05.007, http://www.sciencedirect.com/science/article/B6T4T-506RN5G-2/2/f5785f9d55583c75ec9917e95a9aeb7d

Wolf M, Wolf U, Choi J, Toronov V, Paunescu L, Michalos A, Gratton E (2003) Fast cerebral functional signal in the 100-ms range detected in the visual cortex by frequency-domain near-infrared spectrophotometry. Psychophysiology 40(4):521–528

Wolf M, Morren G, Haensse D, Karen T, Wolf U, Fauchère J, Bucher H (2008) Near infrared spectroscopy to study the brain: an overview. Opto-Electron Rev 16(4):413–419

Zhao H, Tanikawa Y, Gao F, Onodera Y, Sassaroli A, Tanaka K, Yamada Y (2002) Maps of optical differential pathlength factor of human adult forehead, somatosensory motor and occipital regions at multi-wavelengths in NIR. Phys Med Biol 47:2075